Soft Matter

PAPER

View Article Online
View Journal | View Issue

Cite this: *Soft Matter*, 2023, **19**, 3273

Temperature-responsive membrane permeability of recombinant fusion protein vesicles†

Jackson Powers and Yeongseon Jang *

Received 23rd January 2023,
Accepted 15th April 2023

DOI: 10.1039/d3sm00096f

rsc.li/soft-matter-journal

In this study, we investigate the changes in the permeability of the recombinant fusion protein vesicles with different membrane structures as a function of solution temperature. The protein vesicles are self-assembled from recombinant fusion protein complexes composed of an mCherry fused with a glutamic acid-rich leucine zipper and a counter arginine-rich leucine zipper fused with an elastin-like polypeptide (ELP). We have found that the molecular weight cut-off (MWCO) of the protein vesicle membranes varies inversely with solution temperature by monitoring the transport of fluorescent-tagged dextran dyes with different molecular weights. The temperature-responsiveness of the protein vesicle membranes is obtained from the lower critical solution temperature behavior of ELP in the protein building blocks. Consequently, the unique vesicle membrane structures with different single-layered and double-layered ELP organizations impact the sensitivity of the permeability responses of the protein vesicles. Single-layered protein vesicles with the ELP domains facing the interior show more drastic permeability changes as a function of temperature than double-layered protein vesicles in which ELP blocks are buried inside the membranes. This work about the temperature-responsive membrane permeability of unique protein vesicles will provide design guidelines for new biomaterials and their applications, such as drug delivery and synthetic protocell development.

Introduction

Nature inspires many researchers to develop innovative soft biomaterials. Vesicles within or outside cells play an important role in the progress of secretion, uptake, and transport of materials.[1] One of the basic properties required for survival of biological cells is semi-permeable membranes and selective permeability. To mimic and imitate this function in synthetic vesicles, liposomes or polymersomes have been developed and modified chemically, physically, or biologically over the last 40 years.[2–7] However, the inherent properties of liposomes, such as low chemical versatility associated with difficulties in post-modification for short molecular weight lipids, often limit the integration of functional proteins and complex control of their functionality.[8–11] Conversely, polymersomes offer versatility to tune their chemistry and functionality but often require acids, alkalis, organic solvents, or chemical conjugations, which hinder their biocompatibility.[8,12–15]

Protein vesicles or proteinosomes, consisting of fully folded, functional globular proteins, have recently attracted attention due to their expected biological properties, including biocompatibility and specific protein activities in vesicle structure, useful for microbioreactors, drug delivery vehicles, and synthetic protocells.[3,16–19] Particularly, globular protein vesicles (GPVs) can be made through self-assembly of recombinant fusion proteins consisting of fully folded, globular proteins and intrinsically disordered polypeptides in benign aqueous environments at room temperature.[16,17] Since this fabrication is favorable to biological molecules and processes, GPVs can offer diverse biochemical functionality and tunability. The building blocks of GPVs are recombinant protein complexes consisting of a hydrophilic globular protein genetically fused to a glutamic acid-rich leucine zipper (globule-Z_E) and an arginine-rich leucine zipper genetically fused to an elastin-like polypeptide (Z_R-ELP).[16,17,20] The complimentary Z_E/Z_R leucine zippers have a high binding affinity ($K_d \approx 10^{-15}$ M),[21] which results in the dimerization of fusion protein constituents as amphiphiles. The modular design of these fusion proteins allows users to decorate the membrane exterior with any fully folded globular protein desired *via* genetic fusion to a Z_E leucine zipper. Since the new GPV was developed by Champion *et al.* in 2014,[16] diverse engineering strategies to control the vesicle size, membrane structure, and structural integrity in physiological conditions have been developed toward more biomedical and biological applications.[19,22,23] Nonetheless, the novelty of this platform necessitates further investigation of their material properties like selective permeability, which motivates the current study.

Department of Chemical Engineering, University of Florida 1006 Center Drive, FL 32669, USA. E-mail: y.jang@ufl.edu

† Electronic supplementary information (ESI) available. See DOI: https://doi.org/10.1039/d3sm00096f

Elastin-like polypeptide (ELP) is a well-known biopolymer with many uses in the field of self-assembled biomaterials, ranging from drug delivery vehicles to tissue scaffolding.[24–29] ELP consists of 25 penta-repeat units of amino acid sequence (VPGXG), where X denotes any amino acid except proline. ELP exhibits lower critical solution temperature (LCST) behavior, undergoing conformational changes from hydrophilic to hydrophobic at temperatures above its critical solution temperature due to rearrangement of hydrogen bonds in the pentapeptide repeat units.[30,31] Such hydrophilic-to-hydrophobic transition of ELPs has been utilized to develop thermally responsive biomaterials in micelles or thin film forms. In GPVs, this hydrophobic collapse renders ELP tails insoluble in aqueous solutions and forms amphiphilic packing units when bound to hydrophilic globular proteins *via* complementary leucine zippers. Since the critical solution temperature for the hydrophilic-to-hydrophobic transition of ELP varies depending on its chain length, concentration,[32] and attached cargo,[33] two types of GPV membrane structures (*i.e.*, single-layered and double-layered) can be achieved by altering self-assembly conditions that dictate the molecular packing parameter.[17]

Herein, we demonstrate the permeability changes of GPVs with different membrane structures as a function of temperature. GPV membrane permeability can be directly manipulated through control of solution temperature based on the LCST behavior of ELP building blocks. Hence, we hypothesized that the different membrane structures of GPVs will alter the temperature responsiveness in terms of permeability. To test this hypothesis, we systematically investigated the membrane permeability of SLVs and DLVs, as a function of temperature (25, 30, 34, and 37 °C), along with their membrane structure and average size. Selective permeability of GPV membranes was characterized through monitoring permeation of different sized molecules with fluorescent tags at various temperatures. We anticipate that the information about membrane permeability and temperature responsiveness of GPVs would offer high potential in many applications, such as thermally triggered drug release or control over encapsulated enzymatic reactions.

Experimental

Materials

This work used two different types of recombinant fusion proteins: Z_R-ELP and mCherry-Z_E. Z_R-ELP is composed of an arginine-rich leucine zipper (Z_R) genetically fused with and elastin-like polypeptide (ELP, $[(VPGVG)_2(VPGFG)(VPGVG)_2]_5$), and mCherry-$Z_E$ is a globular red fluorescent protein genetically fused with a glutamic acid rich leucine zipper (Z_E). The expression and purification steps of Z_R-ELP and mCherry-Z_E are described in detail in the previous works.[16] The size and purity of the purified proteins were analyzed by SDS-PAGE. Fluorescent dyes used for encapsulation include calcein (ChemCruz), azadibenzocyclooctyne-cyanine 5 (DBCO-Cy5) (Aldrich), coumarin (Acros Organics), fluorescein sodium salt (Sigma), rhodamine B (octadecyl ester perchlorate) (RhoB-OEP) (Chemodex).

GPV formation by self-assembly

GPVs were prepared through mixing fusion proteins in a molar ratio of 0.05 (mCherry-Z_E to Z_R-ELP) at concentrations of 60 μM or 120 μM Z_R-ELP to form single or double layered membranes, respectively. All Z_R-ELP protein is dissolved in 18 MΩ cm^{-1} Milli-Q water, and all mCherry-Z_E is dissolved in 1× phosphate buffered saline (PBS). All solutions were mixed by pipette and incubated for 15 minutes on ice. The fusion protein mixtures were then incubated at 25 °C for one hour in a temperature controlled digital incubator (H2200-HC, Benchmark Scientific).

GPV size and morphology characterization by DLS and microscopy

The hydrodynamic diameter (D_H (nm)) of the self-assembled vesicles was measured by dynamic light scattering (DLS) (Zetasizer Nano ZS, Malvern Instruments). A 4 mW He–Ne laser operating at a wavelength of 633 nm was equipped in the DLS instrument and operated at a detection angle of 173° at temperatures from 25 °C to 45 °C. Each 100 μL sample was prepared in a microcuvette for DLS characterization. The morphology of the protein vesicles was monitored using epifluorescence and confocal microscopes under a 100× oil objective lens (Axio Observer 7, LSM700, Carl Zeiss).

Dye encapsulation into GPVs

All dye encapsulations were performed through addition of fluorescent dyes during the initial 15 min incubation period on ice. 1 μL of dye stock solution in a concentration of 1 mg mL^{-1} was added to 99 μL vesicle solution for all dye encapsulations to achieve a final dye concentration of 10 μg mL^{-1}. Hydrophilic fluorescein sodium salt, coumarin, calcein, and Cy5 were dissolved in water, whereas hydrophobic RhoB-OEP was dissolved in chloroform.

Fluorescence permeability assays

Fluorescence permeability assays were conducted using fluorescein isothiocyanate dextran (FITC-Dextran, Sigma) conjugated fluorescent dyes with dextran at different molecular weights of 4 kDa, 10 kDa, 40 kDa, and 250 kDa. All the data with 250 kDa was not reported as it is not permeable to GPVs in all conditions tested in this work. We confirmed molecular weight cut off (MWCO) of both SLVs and DLVs are smaller than 40 kDa at the temperature ranges we investigated. Additionally, fluorescein disodium salt with molecular weight of 376.3 Da was used to monitor permeation of 0.4 kDa molecules. To test fluorescence permeability, protein vesicles were prepared as described above then incubated at the target temperature (25 °C, 30 °C, 34 °C, 37 °C) for one hour. 1 μL of FITC-Dextran dyes at a concentration of 0.04 M were added to the 100 μL GPV solution and incubated at the target temperature for 10 minutes. The GPV solutions were then imaged on the epifluorescent microscope (Axio Observer 7, Carl Zeiss) and analyzed using the Zen blue built-in fluorescence intensity profile tool. All graphical elements were prepared using Igor Pro.

Transmission electron microscopy (TEM)

TEM samples were prepared using the negative staining agent, phosphotungstic acid (Sigma-Aldrich). 5 μL of sample were loaded onto a carbon film-coated TEM grid (300 MESH, Electron Microscopy Sciences) and left to settle for 15 minutes at the target temperature. The solution was then removed *via* blotting with filter paper and washed twice using Milli-Q water. 5 μL of a 0.5% PTA solution was placed on the grid for 10 seconds. The staining agent was then removed *via* filter paper and the grid was washed twice using Milli-Q water, followed by drying at the target temperature for 24 hours. All images were captured at room temperature using a FEI SPIRIT 120 kV TEM.

Results and discussion

Jang *et al.* previously demonstrated that temperature and concentration can tune the self-assembly of the mCherry-Z_E and Z_R-ELP fusion protein complexes and enable formation of either single-layered or double-layered GPVs.[17] Herein, we characterized the dye encapsulation capabilities of GPVs with two different membrane configurations (single layered vesicles (SLVs) and double layered vesicles (DLVs)) using a diverse range of dyes with different hydrophilicity. We mixed dyes with mCherry-Z_E and Z_R-ELP protein solutions at 4 °C (in soluble phase below the critical solution temperature) and induced vesicle assembly by warming the solution to 25 °C (above the critical solution temperature) to characterize where the dyes locate.

Fig. 1 clearly shows the different membrane structures of SLVs and DLVs. Both SLVs and DLVs can encapsulate hydrophilic or relatively water-soluble dyes (*i.e.*, fluorescein sodium salt, coumarin, calcein, and Cy5) in the water-filled lumen. GPVs are also capable of encapsulating hydrophobic dyes; in fact, addition of hydrophobic rhodamine B octadecyl ester perchlorate (RhoB-OEP) dyes confirmed the different structural organizations of hydrophobic ELP domains in SLVs and DLVs. DLVs encapsulate hydrophobic RhoB-OEP within the vesicle membrane where ELP tails are buried, whereas SLVs encapsulate the hydrophobic dyes sequestered in the vesicle lumen.

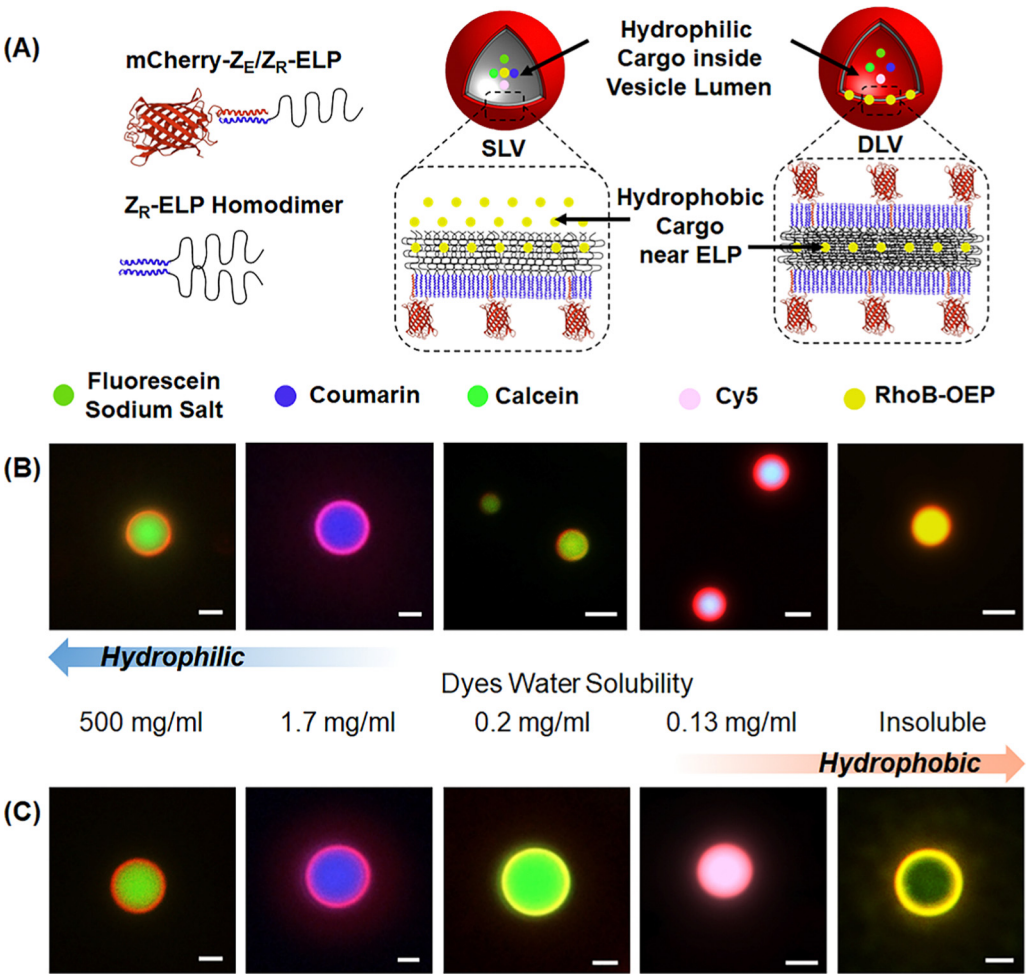

Fig. 1 (A) Schematic illustration showing recombinant fusion protein building blocks for membrane construction of single-layered vesicles (SLVs) and double-layered vesicles (DLVs), along with the locations of encapsulated hydrophilic and hydrophobic cargo. (B and C) Fluorescent micrographs showing encapsulation of diverse fluorescent dyes with different water solubility (fluorescein sodium salt, coumarin, calcein, Cy5, rhodamine B (octadecyl ester perchlorate) (RhoB-OEP)) in (B) SLVs and (C) DLVs. All scale bars are 2 μm.

SLVs have a hydrophobic ELP interface with the water-filled vesicle lumen but still retain hollow vesicle structures due to the steric hindrance of mCherry-Z_E head groups and stiff Z_E/Z_R modules at the surface, preventing SLV collapse to micellar structure.[16] Previous work clearly demonstrated that hollow vesicle structure is made in the single-layered membrane configuration (as shown in Fig. 1A) by several characterization techniques including scanning electron microscopy, transmission electron microscopy, confocal microscopy, and small angle neutron scattering.[16,17] This unique single-layered membrane structure of SLVs, having hydrophobic ELP tails exposed to the water-filled vesicle lumen, enables encapsulation of both hydrophilic and hydrophobic cargo inside the lumen.

The dye encapsulation experiments provided a basis for selecting dyes for permeability studies, which should be encapsulated into the water-filled lumens of both SLVs and DLVs with clear fluorescent signal detection distinguished from red fluorescent mCherry. Since water-soluble fluorescein dyes fulfilled the requirements, we performed membrane permeability assays with fluorescein derivates conjugated with dextrans at different molecular weights (*e.g.*, fluorescein at 0.4 kDa, FITC-dextrans at 4 kDa, 10 kDa, 40 kDa, and 250 kDa).

To confirm temperature-induced permeability changes of GPVs, we added water-soluble fluorescein (0.4 kDa) to pristine SLV vesicle solutions at 25 °C and 37 °C (Fig. 2A). We then monitored the transport of the dyes from the surrounding solution to the vesicle lumen through the membrane. Fig. 2B shows that SLVs at 25 °C allow transport of 0.4 kDa fluorescein dyes across the membrane; however, the membrane becomes impermeable to the same dye at 37 °C. These results indicate that the further hydrophobic collapse of ELP at higher temperatures mitigates the transport of materials across the vesicle membrane. The thermally induced inverse phase transition temperature of ELP can be defined as the temperature where ELP transitions from soluble to insoluble in aqueous solutions. This transition temperature is typically characterized by the temperature at which the optical density drastically increases in the turbidity profile. The transition happened around 20 °C in the SLV assembly condition (Fig. 2C). Since increasing the temperature further above the transition temperature can induce a tighter hydrophobic collapse of ELP, we attribute the decreased membrane permeability of SLVs at 37 °C as compared to 25 °C to this further hydrophobic collapse.

In order to estimate molecular weight cut off (MWCO) of SLVs and DLVs, we repeated the dye permeability assays by monitoring the transport of fluorescein derivates with dextrans at different molecular weights (*i.e.*, 0.4 kDa, 4 kDa, 10 kDa, 40 kDa, 250 kDa) and different solution temperatures (25 °C, 30 °C, 34 °C, and 37 °C). GPV membranes are considered permeable to a specific-sized dye when the dye is observed to diffuse across the membrane from outside to inside. By monitoring the fluorescent signals within the vesicle lumen at the target temperature, the MWCO for GPVs can be defined as the molecular weight of the fluorescent dye at which transport through the GPV membrane begins to be blocked at each respective temperature. For example, Fig. 3 shows MWCO of

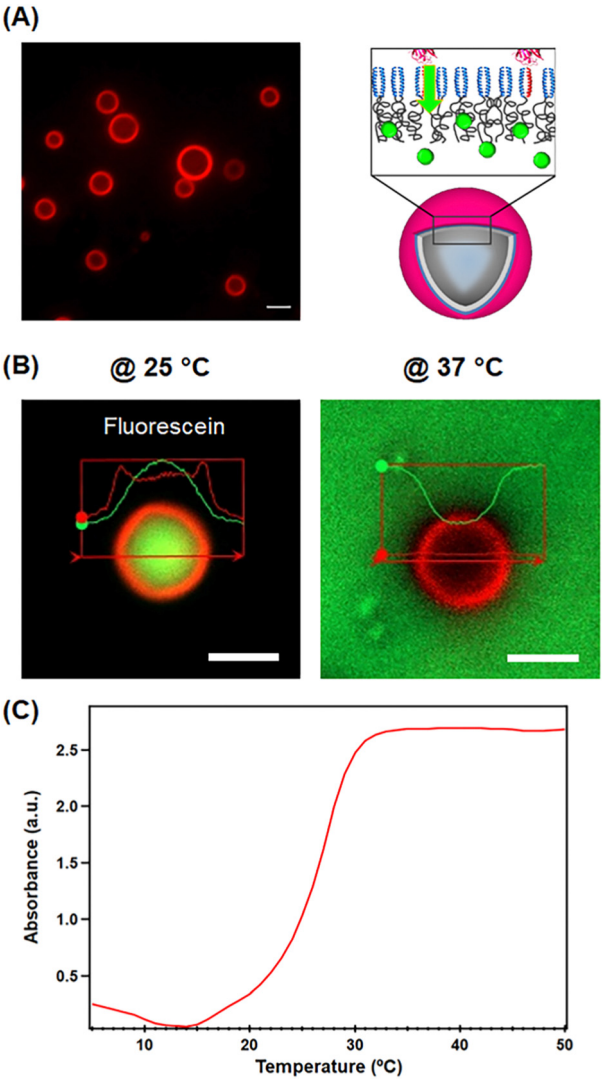

Fig. 2 (A) A fluorescent micrograph of pristine SLVs at 25 °C and a scheme to show the transport of dye molecules through the membrane, (B) fluorescent micrographs of SLVs upon addition of fluorescein at 25 °C (left) and at 37 °C (right). Inset profiles indicate red and green fluorescent intensity from mCherry and fluorescein, respectively. All inset scale bars are 2 μm. (C) Turbidity profile of a SLV solution, measured by UV absorbance at 400 nm wavelength, as a function of temperature. The heating rate is 1 °C min^{-1}.

SLVs at 25 °C is between 10 kDa and 40 kDa, as FITC-Dextrans with less than 10 kDa molecular weights can permeate through SLVs while 40 kDa and 250 kDa cannot. The vesicles that show green fluorescence inside overlapped with red rings indicate the mCherry-assembled vesicle membrane is permeable to 4 kDa and 10 kDa FITC-dextrans (Fig. 3A and B). On the other hand, the red fluorescence only inside of the vesicles implies a lack of 40 kDa and 250 kDa FITC-dextrans (Fig. 3C and D) due to limited transport into the membranes. In this regard, we defined the MWCO of SLVs at 25 °C as 40 kDa.

It is worth noting that more precise control over the molecular weights of transport molecules would be necessary to accurately characterize the MWCO of semi-permeable GPVs,

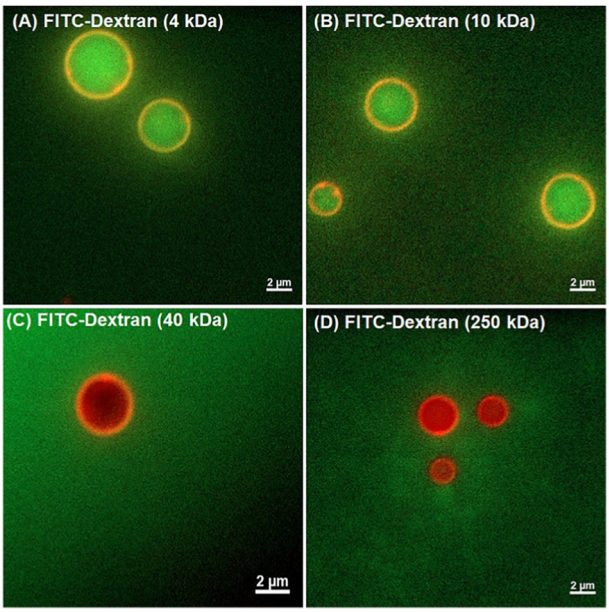

Fig. 3 Fluorescent micrographs of SLVs at 25 °C show selective permeability of dyes depending on size. (A) 4 kDa and (B) 10 kDa FITC-dextrans are able to permeate SLV membranes made of mCherry-Z_E/Z_R-ELP, whereas (C) 40 kDa and (D) 250 kDa are not.

which is beyond the scope of our current study. More interestingly, we found that the configuration of the membrane structure of GPVs influenced the magnitude of the temperature-induced permeability changes. As a result, the MWCO of SLVs shows stronger dependence on solution temperature than DLVs. We summarized the largest FITC-Dextran that is able to permeate the membrane and the next largest FITC-Dextran that is unable to permeate the membrane, assigned MWCO in this work, for both SLVs and DLVs at each temperature in Fig. 4.

Specifically, green fluorescence from FITC-dextrans inside red fluorescent GPVs indicates that the membranes are permeable for the specific-sized dyes to transport from outside into the lumen (permeable; upper rows in Fig. 4A and B, respectively). When the membranes become permeable to the dyes, both SLVs and DLVs exhibit a unique phenomenon in which dyes diffuse uphill. When fluorescent dyes are added to the solution surrounding the vesicles, they first diffuse into the lumen following the concentration gradient, then past equilibrium, and continue to diffuse against the concentration gradient to achieve a higher concentration inside the vesicles than outside. Uphill diffusion has been described in mixtures that contain multiple components, where the diffusion of one species is closely linked to that of its partner species.[34] GPVs are self-assembled from fusion protein complexes, and the vesicle membranes contain multiple protein domains that can potentially impact the diffusion of dyes *via* specific interactions. This result indicates that passive diffusion is not the only process governing the transport of dyes across the membrane.

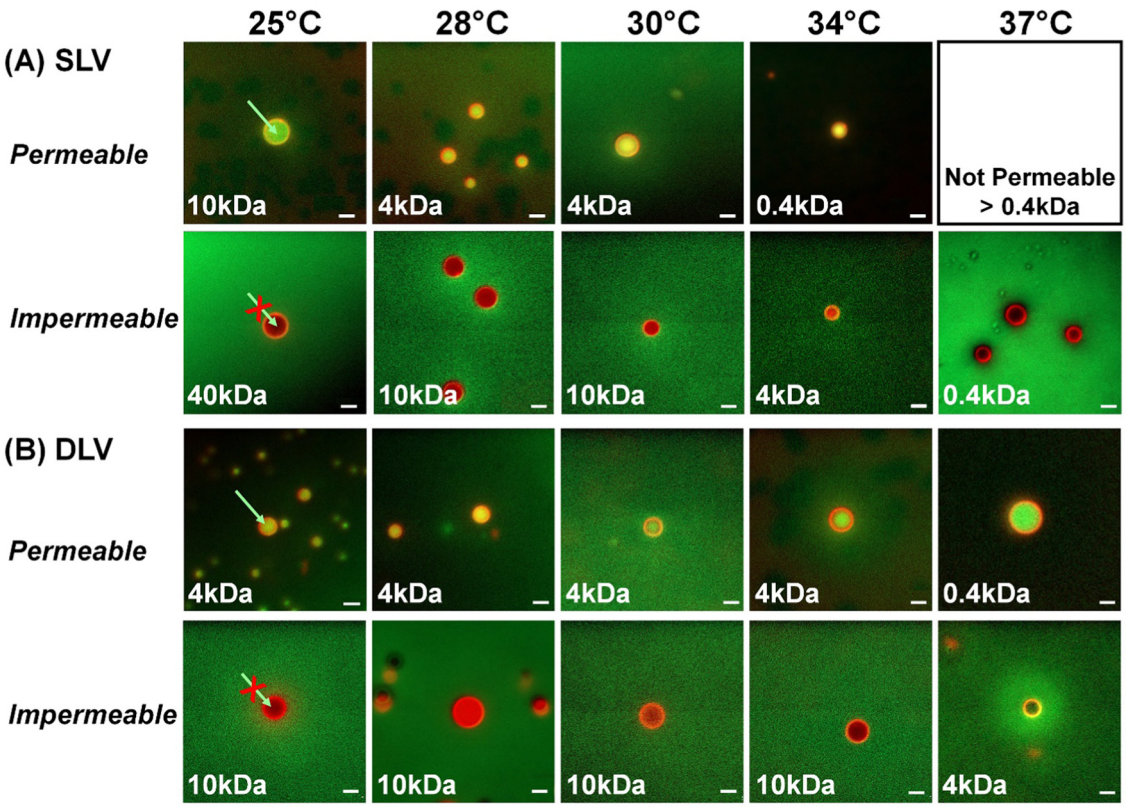

Fig. 4 Fluorescent micrographs of (A) SLVs and (B) DLVs show the MWCOs at temperatures between 25 °C and 37 °C upon addition of variable molecular weight FITC-dextran. The largest MW FITC-dextran that is able to permeate the membrane is shown in the upper rows, and the next largest dye that is unable to permeate the membrane, assigned MWCO, in this work is shown in the lower rows at each temperature. All inset scale bars are 2 μm.

Therefore, we anticipate that other factors in addition to the coupled diffusion effect may contribute to the driving force for uphill diffusion. Nevertheless, it is obvious that SLVs show more drastic changes in the dye sizes that can pass through the membranes, with respect to temperature, as compared to DLVs. When the GPV membranes are impermeable to FITC-dextrans at given temperatures (impermeable; lower rows in Fig. 4A and B, respectively) green fluorescent signal from the dyes is not observed inside the vesicle lumen.

We attribute the unique dye diffusion behavior and different thermal responses of SLVs and DLVs, which dictate membrane permeability, to different ELP layer organizations. Several attempts have been made to model the precise mechanism behind the temperature responsive behavior and structural transitions of ELP;[31] however, the field does not yet agree on one defined mechanism. Additionally, ELP-ELP association in different self-assembled structures warrants future investigation. Therefore, we highlight the first report to our best knowledge, demonstrating that the SLVs span a wide range of MWCOs as a function of solution temperature, from 40 kDa at 25 °C to less than 0.4 kDa at 37 °C, whereas DLVs exhibit a smaller range of permeability changes than SLVs, from 10 kDa at 25 °C to 4 kDa at 37 °C, over the same temperature window (Fig. 5).

It is thought that the decrease in the ELP transition temperature for DLV conditions (~15 °C), compared with SLV (~20 °C), resulted in less responsiveness to the thermal gating in the temperature window from 25 °C to 37 °C. We compared the transition temperatures of ELPs in SLVs and DLVs from the optical density profiles. We defined the transition temperature as the temperature at which the turbidity began to increase rapidly, indicating that soluble to insoluble transition in aqueous solutions (Fig. S1 in ESI†). As a result, we anticipate that the ELP domain is predominately responsible for the temperature-responsive changes in permeability of GPVs as the other membrane components have no known temperature response over the temperatures tested. Thus, the increase in hydrophobic interactions between the ELP domains upon further increase of the temperature above the critical solution temperature reduces the membrane permeability with tighter membrane association and increased hydrophobicity against water soluble dyes for both SLVs and DLVs with different sensitivities.

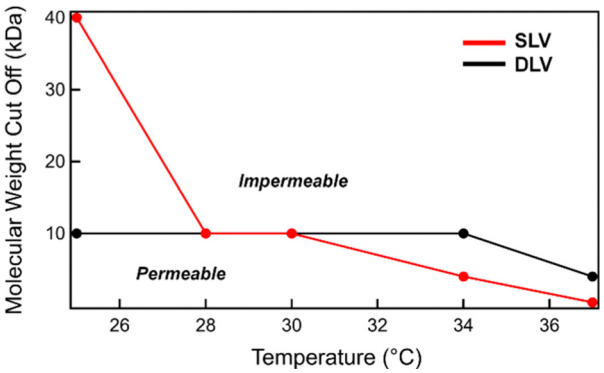

Fig. 5 Graphical representation of the MWCO of SLVs (red) and DLVs (black) with respect to the temperature.

We also attribute the difference in temperature response between the two membrane configurations to the presence of an ELP–water interface. As previously discussed, the rigid, rod-shaped conformation of the leucine zippers and the steric hinderance of the mCherry domains can maintain the hollow structure of SLVs with the structural configuration of hydrophilic mCherry-Z_E/Z_R at the surface and hydrophobic ELP faced towards the water filled lumen.[16,17] In this unique SLV structure, the increase of ELP hydrophobic collapse upon warming is predicted to allow lateral contraction of protein building blocks throughout the membrane as it increases phase separation of ELPs in water. We predict that the mechanisms to explain these changes in permeability of SLVs are analogous to the mechanisms used in literature to explain the cargo release of thermo-responsive micelles. The immiscibility of hydrophilic arms and hydrophobic cores of building blocks induce micellization while encapsulating hydrophobic cargo inside. On the other hand, the reduction of hydrophobicity in the hydrophobic cores of micelles leads to swelling or disassembly of the micelle to increase the permeability while also allowing the release of encapsulants.[35,36] In this way, lowering temperature results in the increase of hydration of ELP domains in SLVs, allowing the lateral swelling of the membrane with increased permeability. Likewise, upon an increase in temperature, the change in membrane association with the tighter binding of ELP laterally and vertically throughout the membrane reduces the space available for large FITC-dextran dyes to permeate. TEM images confirmed that SLVs retain hollow vesicle structures at 25 °C and 37 °C (Fig. S2 in ESI†).

In DLVs, similar to traditional liposomes and polymersomes, hydrophobic RhoB-OEP is trapped within the membrane and hydrophilic dyes are sequestered in the water-rich vesicle lumen. This proves that DLVs have a bilayer membrane structure where the hydrophobic ELP domains face each other on the interior of the membrane and the hydrophilic mCherry and leucine zipper exist at the outer and inner vesicle surfaces. Thus, we expect that the lack of an ELP-water interface and steric hindrance between globular proteins at both surface sides limit the lateral rearrangement of ELP but allow its hydrophobic collapse in the direction normal to the membrane upon increases in temperature. Also, the ELP domains are thought to be more densely packed and have a higher degree of hydrophobicity in double layered membranes, resulting in smaller MWCO of DLVs (~10 kDa) than SLVs (~40 kDa) at 25 °C. The more densely packed membrane of DLVs sterically hinders the permeation of dyes across the membrane. Upon increase of temperature, MWCOs of DLVs were not significantly altered as compared to SLVs. We anticipate that the slight decrease of permeability of DLVs at higher temperature (from MWCO of 10 kDa at 25 °C to 4 kDa at 37 °C) is induced from more compact packing of the membranes with ELP hydrophobic collapse in normal direction coupled with a slight decrease in solvation of the ELP tails. Similarly, it was reported that the

increased packing of lipid molecules decreases the permeability coefficient in liposomes.[37] Furthermore, recent report of polymer–peptide and lipid–peptide vesicle membranes, which undergo changes in membrane permeability in response to the secondary structure transitions of hydrophobic peptides, support our results.[38,39]

Conclusion

Herein, we have demonstrated the unique thermal gating properties of GPVs owing to the LCST behavior of the hydrophobic ELP domains in the vesicle membrane. Through comprehensive fluorescent dye permeability assays, we have characterized the thermally induced permeability changes of two different types of GPV membrane configurations. The results revealed a higher sensitivity to thermal gating in a single-layered configuration, which is the unique structure found in GPV platforms, than in a double-layered vesicle. While identifying the rearrangement of fusion proteins and associated membrane structure changes in GPVs at the molecular level warrants future investigations with other experimental and computational methods, this is the first report, to our best knowledge, of tunable membrane permeability of protein vesicles in two different types of self-assembled membrane configurations. Furthermore, various functional proteins can be substituted in GPVs by designing fusion protein building blocks through potential recombinant protein technology. Our findings in this work would enable the introduction of a range of permeability modulation over a small temperature control range in diverse GPV platforms, including other functional protein constituents. The effect of temperature and membrane configuration of ELP in potential GPVs would also provide critical information to develop new biomaterials and applications, such as drug delivery and synthetic protocells.

Author contributions

The manuscript was written through contributions from all authors. J. P. designed and performed all experiments and Y. J. supervised data analysis and manuscript writing. All authors have given approval to the final version of the manuscript.

Conflicts of interest

There are no conflicts to declare.

Acknowledgements

This work has been financially supported by the National Science Foundation (NSF), CBET CAREER Award (Grant No. 2045313) and MCB (Grant No. 2123592). We acknowledge Prof. Julie A. Champion (Georgia Institute of Technology) for graciously providing genetic information. encoding fusion proteins mCherry-Z_E and Z_R-ELP, plasmids, and cells.

References

1 N. A. Yewdall, A. F. Mason and J. C. M. van Hest, The hallmarks of living systems: towards creating artificial cells, *Interface Focus*, 2018, **8**(5), 20180023.
2 L. Olivi, M. Berger, R. N. P. Creyghton, N. De Franceschi, C. Dekker, B. M. Mulder, N. J. Claassens, P. R. ten Wolde and J. van der Oost, Towards a synthetic cell cycle, *Nat. Commun.*, 2021, **12**(1), 4531.
3 X. Huang, M. Li, D. Green, D. Williams, A. Patil and S. Mann, Interfacial assembly of protein-polymer nanoconjugates into stimulus-responsive biomimetic protocells, *Nat. Commun.*, 2013, **4**, 2239.
4 S. Deshpande, W. K. Spoelstra, M. van Doorn, J. Kerssemakers and C. Dekker, Mechanical Division of Cell-Sized Liposomes, *ACS Nano*, 2018, **12**(3), 2560–2568.
5 M. Weiss, J. P. Frohnmayer, L. T. Benk, B. Haller, J.-W. Janiesch, T. Heitkamp, M. Börsch, R. B. Lira, R. Dimova, R. Lipowsky, E. Bodenschatz, J.-C. Baret, T. Vidakovic-Koch, K. Sundmacher, I. Platzman and J. P. Spatz, Sequential bottom-up assembly of mechanically stabilized synthetic cells by microfluidics, *Nat. Mater.*, 2018, **17**(1), 89–96.
6 K. P. Adamala, D. A. Martin-Alarcon, K. R. Guthrie-Honea and E. S. Boyden, Engineering genetic circuit interactions within and between synthetic minimal cells, *Nat. Chem.*, 2017, **9**(5), 431–439.
7 B. Drobot, J. M. Iglesias-Artola, K. Le Vay, V. Mayr, M. Kar, M. Kreysing, H. Mutschler and T. Y. D. Tang, Compartmentalised RNA catalysis in membrane-free coacervate protocells, *Nat. Commun.*, 2018, **9**(1), 3643.
8 E. Rideau, R. Dimova, P. Schwille, F. R. Wurm and K. Landfester, Liposomes and polymersomes: a comparative review towards cell mimicking, *Chem. Soc. Rev.*, 2018, **47**(23), 8572–8610.
9 P. Nakhaei, R. Margiana, D. O. Bokov, W. K. Abdelbasset, M. A. Jadidi Kouhbanani, R. S. Varma, F. Marofi, M. Jarahian and N. Beheshtkhoo, Liposomes: Structure, Biomedical Applications, and Stability Parameters With Emphasis on Cholesterol, *Front. Bioeng. Biotechnol.*, 2021, **9**, 705886.
10 J.-L. Rigaud and D. Lévy, Reconstitution of Membrane Proteins into Liposomes, *Methods in Enzymology*, Academic Press, 2003, vol. 372, pp. 65–86.
11 A. Akbarzadeh, R. Rezaei-Sadabady, S. Davaran, S. W. Joo, N. Zarghami, Y. Hanifehpour, M. Samiei, M. Kouhi and K. Nejati-Koshki, Liposome: classification, preparation, and applications, *Nanoscale Res. Lett.*, 2013, **8**(1), 102.
12 N. Aibani, T. N. Khan and B. Callan, Liposome mimicking polymersomes; A comparative study of the merits of polymersomes in terms of formulation and stability, *Int. J. Pharm.: X*, 2020, **2**, 100040.
13 P. V. Pawar, S. V. Gohil, J. P. Jain and N. Kumar, Functionalized polymersomes for biomedical applications, *Polym. Chem.*, 2013, **4**(11), 3160–3176.
14 S. Egli, M. G. Nussbaumer, V. Balasubramanian, M. Chami, N. Bruns, C. Palivan and W. Meier, Biocompatible Functionalization of Polymersome Surfaces: A New Approach to

Surface Immobilization and Cell Targeting Using Polymersomes, *J. Am. Chem. Soc.*, 2011, **133**(12), 4476–4483.
15 O. Rifaie-Graham, S. Ulrich, N. F. B. Galensowske, S. Balog, M. Chami, D. Rentsch, J. R. Hemmer, J. Read de Alaniz, L. F. Boesel and N. Bruns, Wavelength-Selective Light-Responsive DASA-Functionalized Polymersome Nanoreactors, *J. Am. Chem. Soc.*, 2018, **140**(25), 8027–8036.
16 W. Park and J. Champion, Thermally Triggered Self-Assembly of Folded Proteins into Vesicles, *J. Am. Chem. Soc.*, 2014, **136**(52), 17906–17909.
17 Y. Jang, W. Choi, W. Heller, Z. Ke, E. Wright and J. Champion, Engineering Globular Protein Vesicles through Tunable Self-Assembly of Recombinant Fusion Proteins, *Small*, 2017, **13**(36), 1700399.
18 Y. Jang, M. Hsieh, D. Dautel, S. Guo, M. Grover and J. Champion, Understanding the Coacervate-to-Vesicle Transition of Globular Fusion Proteins to Engineer Protein Vesicle Size and Membrane Heterogeneity, *Biomacromolecules*, 2019, **20**(9), 3494–3503.
19 R. Tan, J. Shin, J. Heo, B. Cole, J. Hong and Y. Jang, Tuning the Structural Integrity and Mechanical Properties of Globular Protein Vesicles by Blending Crosslinkable and Non-Crosslinkable Building Blocks, *Biomacromolecules*, 2020, **21**(10), 4336–4344.
20 Y. Jang and J. A. Champion, Self-Assembled Materials Made from Functional Recombinant Proteins, *Acc. Chem. Res.*, 2016, **49**(10), 2188–2198.
21 J. R. Moll, S. B. Ruvinov, I. Pastan and C. Vinson, Designed heterodimerizing leucine zippers with a ranger of pIs and stabilities up to 10(-15) M, *Protein Sci.*, 2001, **10**(3), 649–655.
22 Y. Li and J. A. Champion, Photocrosslinked, Tunable Protein Vesicles for Drug Delivery Applications, *Adv. Healthc. Mater.*, 2021, **10**(15), e2001810.
23 D. R. Dautel, W. T. Heller and J. A. Champion, Protein Vesicles with pH-Responsive Disassembly, *Biomacromolecules*, 2022, **23**(9), 3678–3687.
24 W. B. Jeon, B. H. Park, J. Wei and R. W. Park, Stimulation of fibroblasts and neuroblasts on a biomimetic extracellular matrix consisting of tandem repeats of the elastic VGVPG domain and RGD motif, *J. Biomed. Mater. Res.*, 2011, **97**(2), 152–157.
25 S. R. MacEwan and A. Chilkoti, Elastin-like polypeptides: biomedical applications of tunable biopolymers, *Biopolymers*, 2010, **94**(1), 60–77.
26 D. H. T. Le and A. Sugawara-Narutaki, Elastin-like polypeptides as building motifs toward designing functional nanobiomaterials, *Mol. Syst. Des. Eng.*, 2019, **4**(3), 545–565.
27 M. S. Desai, M. Chen, F. H. J. Hong, J. H. Lee, Y. Wu and S.-W. Lee, Catechol-Functionalized Elastin-like Polypeptides as Tissue Adhesives, *Biomacromolecules*, 2020, **21**(7), 2938–2948.
28 Y.-N. Zhang, R. K. Avery, Q. Vallmajo-Martin, A. Assmann, A. Vegh, A. Memic, B. D. Olsen, N. Annabi and A. Khademhosseini, A Highly Elastic and Rapidly Crosslinkable Elastin-Like Polypeptide-Based Hydrogel for Biomedical Applications, *Adv. Funct. Mater.*, 2015, **25**(30), 4814–4826.
29 J. J. Milligan, S. Saha, I. C. Jenkins and A. Chilkoti, Genetically encoded elastin-like polypeptide nanoparticles for drug delivery, *Curr. Opin. Biotechnol*, 2022, **74**, 146–153.
30 N. K. Li, F. G. Quiroz, C. K. Hall, A. Chilkoti and Y. G. Yingling, Molecular Description of the LCST Behavior of an Elastin-Like Polypeptide, *Biomacromolecules*, 2014, **15**(10), 3522–3530.
31 N. K. Li, Y. Xie and Y. G. Yingling, Insights into Structure and Aggregation Behavior of Elastin-like Polypeptide Coacervates: All-Atom Molecular Dynamics Simulations, *J. Phys. Chem. B*, 2021, **125**(30), 8627–8635.
32 D. E. Meyer and A. Chilkoti, Quantification of the Effects of Chain Length and Concentration on the Thermal Behavior of Elastin-like Polypeptides, *Biomacromolecules*, 2004, **5**(3), 846–851.
33 K. Trabbic-Carlson, D. E. Meyer, L. Liu, R. Piervincenzi, N. Nath, T. LaBean and A. Chilkoti, Effect of protein fusion on the transition temperature of an environmentally responsive elastin-like polypeptide: a role for surface hydrophobicity?, *Protein Eng., Des. Sel.*, 2004, **17**(1), 57–66.
34 R. Krishna, Uphill diffusion in multicomponent mixtures, *Chem. Soc. Rev.*, 2015, **44**(10), 2812–2836.
35 Y. Tang, S. Y. Liu, S. P. Armes and N. C. Billingham, Solubilization and Controlled Release of a Hydrophobic Drug Using Novel Micelle-Forming ABC Triblock Copolymers, *Biomacromolecules*, 2003, **4**(6), 1636–1645.
36 J. E. Chung, M. Yokoyama, M. Yamato, T. Aoyagi, Y. Sakurai and T. Okano, Thermo-responsive drug delivery from polymeric micelles constructed using block copolymers of poly(N-isopropylacrylamide) and poly(butylmethacrylate), *J. Controlled Release*, 1999, **62**(1–2), 115–127.
37 J. Frallicciardi, J. Melcr, P. Siginou, S. J. Marrink and B. Poolman, Membrane thickness, lipid phase and sterol type are determining factors in the permeability of membranes to small solutes, *Nat. Commun.*, 2022, **13**(1), 1605.
38 Y. Zheng, Z. Wang, Z. Li, H. Liu, J. Wei, C. Peng, Y. Zhou, J. Li, Q. Fu, H. Tan and M. Ding, Ordered Conformation-Regulated Vesicular Membrane Permeability, *Angew. Chem., Int. Ed.*, 2021, **60**(41), 22529–22536.
39 V. Ibrahimova, H. Zhao, E. Ibarboure, E. Garanger and S. Lecommandoux, Thermosensitive Vesicles from Chemically Encoded Lipid-Grafted Elastin-like Polypeptides, *Angew. Chem., Int. Ed.*, 2021, **60**(27), 15036–15040.

